

From thermal creeping to thermal weakening: How crushing plastic and unrolling tape unravels fracture physics

Tom Vincent-Dospital,^{1,2,*} Renaud Toussaint,^{1,2,†} Stéphane Santucci,^{3,4} Loïc Vanel,⁵ Daniel Bonamy,⁶ Lamine Hattali,⁷ Alain Cochard,¹ Eirik G. Flekkøy,² and Knut Jørgen Måløy²

¹*Institut de Physique du Globe de Strasbourg, UMR 7516 CNRS, Université de Strasbourg/EOST, France*

²*SFF Porelab, The Njord Centre, Department of physics, University of Oslo, Norway*

³*Laboratoire de Physique, ENS Lyon, France*

⁴*Mechanics of disordered media laboratory, Lavrentyev Institute of Hydrodynamics of the Russian Academy of Science*

⁵*University of Lyon, Université Claude Bernard Lyon 1, CNRS, Institut Lumière Matière, F-69622, VILLEURBANNE, France*

⁶*Service de Physique de l'Etat Condensé, CEA, CNRS, Université Paris-Saclay, CEA Saclay, 91191 Gif-sur-Yvette Cedex, France*

⁷*Laboratoire FAST, UMR 7608 CNRS, Université Paris-Sud, France*

(Dated: September 2, 2022)

While of paramount importance in material science and engineering, the rupture of solids is often described by empirical observations rather than by fully understood physical models. The earliest formalism is probably that by Griffith¹: the propagation of cracks is described as a threshold phenomenon, only obtained when fractures are loaded above a critical fracture energy. This view matches the behaviour of brittle matter, which suddenly snaps passed a certain elastic deformation. It is however acknowledged that a crack loaded below the mentioned threshold is still growing, but at rates that are orders of magnitude below that of a ‘dynamic’ fracture. One possible approach is to consider that the fracture energy is dependent on the propagation velocity^{2,3}, rather than being a strict medium property. Alternatively, these slow creep regimes are well modelled by thermally activated sub-critical laws such as Arrhenius-like growth rate⁴⁻⁸. It was suggested⁹ that the description of both the slow and the fast regimes, as well as that of the threshold phenomena, could be unified if accounting for the plasticity around the crack tip¹⁰, in particular as the associate induced heat might locally soften the matter^{11,12}. We here propose a unifying model which neglects such an effect of the thermal dissipation, but focuses instead on how temperature affects the front sub-critical growth. We show how this model accounts for experimental data gathered during the failure of two different materials, at all velocities over eight orders of magnitude, thus shedding new light on fracture physics.

We consider that the velocity V of cracks is ruled by the competition, at their tips, between breaking and healing processes^{8,15}, both following an Arrhenius law. The

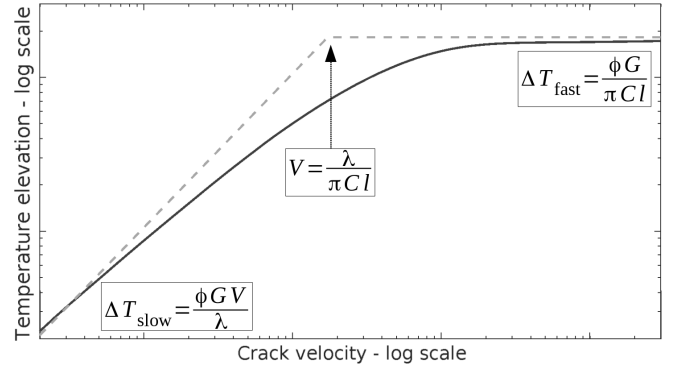


FIG. 1. Steady thermal elevation at a crack tip for various propagation velocity, as per Eq. (2) (plain plot). Approximations ΔT_{fast} and ΔT_{slow} are shown for comparison (dotted plots). Axes are unlabelled for the sake of generality.

activation energy of these laws is modelled proportional to the difference between the energy release rate G (in J m^{-2}) and the intrinsic energy barriers for breaking and healing the atomic bonds of a surface unit, G_c and G_h . While G arises from the mechanical load on the fracture, G_c and G_h are media properties (i.e., notably independent of the propagation velocity). Such a model defines the velocity as:

$$V = V_0 \left[\exp \left(-\frac{\alpha^2(G_c - G)}{k_B(T_0 + \Delta T)} \right) - \exp \left(-\frac{\alpha^2(G_h + G)}{k_B(T_0 + \Delta T)} \right) \right] \quad \text{when } G < G_c$$

$$V = V_0 \left[1 - \exp \left(-\frac{\alpha^2(G_h + G)}{k_B(T_0 + \Delta T)} \right) \right] \quad \text{when } G \geq G_c, \quad (1)$$

where α^2 is an area associated with the active atomic links, k_B is Boltzmann’s constant, and V_0 the thermal bath molecular velocity, typically in the order of the Rayleigh velocity in the medium¹⁶. We also assume that a fraction ϕ of the mechanical energy is dissipated into heat in a process zone^{10,17,18} of radius l around the

* vincentdospitalt@unistra.fr

† renaud.toussaint@unistra.fr

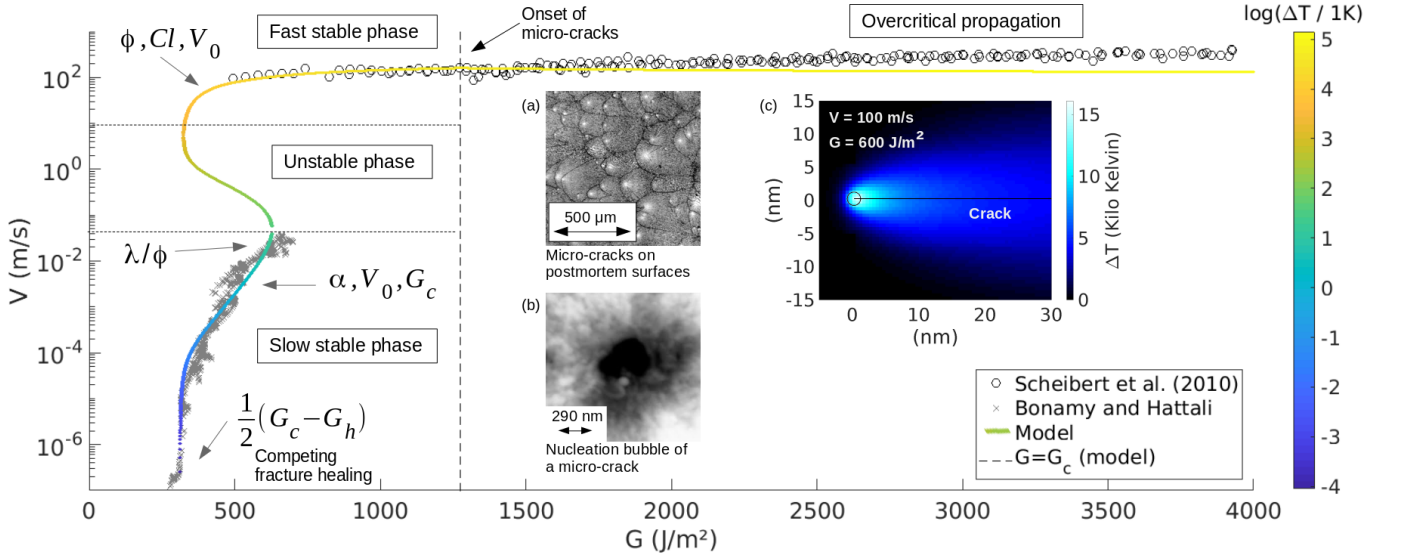


FIG. 2. Crack velocity V as a function of the energy release rate G as predicted by Eq. (1) and (2) and fitted to the PMMA experimental data^{13,14}. The arrows indicate which model parameters each part of the curve is mainly sensitive to. (a): Fractography of secondary micro-cracks on a postmortem fracture surface¹³. White areas mark their nucleation centres. (b): Atomic Force Microscopy of a cavity at the centres of micro-cracks. (c): Modelled temperature field around the crack front, for $V \sim 100 \text{ m s}^{-1}$ and $G \sim 600 \text{ J m}^{-2}$. The circle corresponds to the tip of radius l .

front, and therefore write the absolute tip temperature as $T_0 + \Delta T$, where T_0 is the ambient temperature and ΔT follows the diffusion equation¹⁸:

$$\frac{\partial(\Delta T)}{\partial t} = \frac{\lambda}{C} \nabla^2(\Delta T) + \frac{\phi G V}{C \pi l^2} f. \quad (2)$$

λ is the medium's thermal conductivity, C is the volumetric heat capacity, and f is the support function of the process zone (i.e., $f = 1$ in it and $f = 0$ otherwise). Note that, by down-scaling G to the actual stress at the crack front, one can derive¹⁹ (see supplementary information) that α and the size l of the heat production zone are related:

$$4\pi l \alpha^2 \sim d_0^3, \quad (3)$$

where d_0 is the scale of an atomic bond ($d_0 \sim 1 \text{ \AA}$), making α an equivalent scale smaller than an ångström. We will however invert α and l separately, not to rely on Eq. (3). The governing equation for ΔT (2) can approximate to far simpler expressions¹⁸, as, at low propagation velocities, the thermal elevation is only governed by the diffusion skin depth upon the passage of the process zone, while, for fast cracks, the extra heat can barely diffuse away and ΔT is constrained by l :

$$\Delta T_{\text{slow}} = \frac{\phi G V}{\lambda}, \quad \Delta T_{\text{fast}} = \frac{\phi G}{\pi C l}. \quad (4)$$

See Fig. 1 for the general evolution of ΔT with V . Solving Eq. (1) and (2) simultaneously and focusing on their steady state, one can show the existence of two stable phases for the crack propagation (See Fig. 2).

The first phase is a slow one as ΔT stays small compared to T_0 , such that the growth rate is mainly governed by the medium toughness. The second phase is reached when the generated heat significantly overcomes the background temperature. The propagation rate significantly increases and the crack is said to be thermally weakened. Both phases coexist for a certain range of energy release rate: a hysteresis situation holds and the model also predicts a third, unstable, phase, unlikely to be recorded experimentally.

Interestingly, this phase description matches key observations of fracturing experiments. The abrupt transition, passed a load threshold, from slow to fast cracks, can indeed be interpreted as a phase transition, and the stick-slip of fronts, when avalanches are bigger than the typical medium's quenched disorder, is a good indicator for hysteresis. Let us first compare our model to data acquired when breaking Poly-methyl methacrylate sheets (PMMA) at room temperature ($T_0 = 296 \text{ K}$). A wedge is forced into Perspex[®] bodies, resulting in cracks for which two stable (G, V) branches are recorded, as shown in Fig. 2. A fast branch, as reported by Scheibert et al.¹³ and a slow one, which is here published for the first time (see supplementary information). When forcing the velocity between these two regimes (i.e., above a specific velocity of 4 cm s^{-1} and below 100 m s^{-1}), some stick-slip is observed²². Figure 2 compares both sets of data with the model, and we now pursue by detailing the fit of each parameter. First, notice the linear $\ln(V)$ to G relationship that holds at low velocity, between 10^{-4} and 10^{-2} m s^{-1} . There, $\Delta T \ll T_0$ and G is high enough for healing

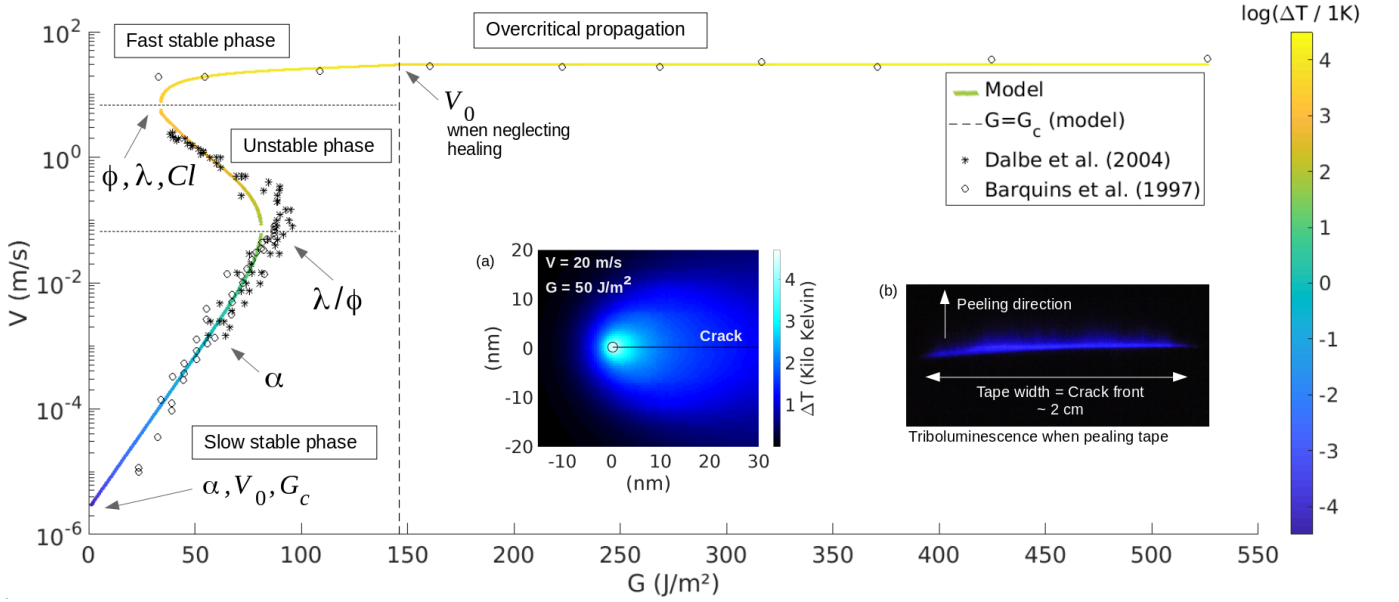


FIG. 3. Crack velocity V as a function of the energy release rate G as predicted by Eq. (1) and (2) and fitted to the tape experimental data^{20,21}. The unstable branch cannot be measured and the data points there are only averaged V versus G for a crack that stick-slips, in the given set-up, between the slow and the fast phase. The arrows indicate to which model parameters each part of the curve is mainly sensitive. (a): Modelled temperature field around the crack front, at the onset of the fast to slow phase shift ($V = 20$ m/s⁻¹). (b): Blue radiation emitted when quickly peeling tape in the dark, as captured by a reflex camera.

processes to be secondary, leading to:

$$\ln(V) = G \left[\frac{\alpha^2}{k_B T_0} \right] + \left[\ln(V_0) - \frac{\alpha^2 G_c}{k_B T_0} \right], \quad (5)$$

where \ln is the natural logarithm. The slope of this data hence constrains α to about 8 pm (indicating $l \sim 1$ nm as per Eq. [3]). Additionally, the intercept of Eq. (5) with the V axis links V_0 and G_c . As we consider the former to be similar to the medium Rayleigh velocity¹³, 880 m/s⁻¹, we deduce $G_c \sim 1275$ J/m². G_h can next be inferred from the asymptote at $G = 300$ J/m², below which healing prevails and cracks cannot propagate. Equation (1) predicts it for $G \sim [G_c - G_h]/2$ such that $G_h \sim 650$ J/m². Let us focus now on the local G maximum, around $V = 4$ cm/s⁻¹. It is modelled by Eq. (1) once ΔT stops being negligible compared to T_0 , which, as per (4), depends on the λ/ϕ ratio. By tuning this ratio, we deduce it to be around 0.9 J s⁻¹ m⁻¹ K⁻¹. As the PMMA conductivity, $\lambda = 0.18$ J s⁻¹ m⁻¹ K⁻¹, is known, we can approximate $\phi \sim 20\%$. Note that this particular point, where $\partial G/\partial V = 0$ and which is directly related to the medium heat conductivity, is the macroscopic critical energy release rate at which the polymer suddenly breaks^{11,23}. We here show how it happens at a value less than the actual microscopic G_c barrier. Lastly, as the crack needs to be hot enough to explain fast fronts at low G (the slower part of the fast branch in Fig. 2), we can estimate the limiting factor of ΔT_{fast} , Cl . Matching the data set in this area, we deduce l to be at most in the nanometer range, which is satisfyingly consistent

with the value inferred from α . We hence predict that most of the induced molecular agitation is introduced on the closest atoms around the crack tip, and, with the discussed parameters, our simple sub-critical model matches most of the rupture dynamics. In Fig. 2 however, a slope break holds passed $G = G_c$, and is not accounted for. At this load, while the crack advances around 165 m/s⁻¹, Guerra et al.¹⁴ showed that micro-cracks start to nucleate ahead of the front (Fig. 2). Although the observed macroscopic speed increases with the growing density of these secondary fronts, the individual velocity of each crack was inferred to stay constant, around 200 m/s⁻¹, that is, compatible with the model. Equation (1) actually explains why the plateau velocity V_{lim} stays below the one of Rayleigh waves: when the tip temperature is high, the healing processes do significantly limit the growth rate. By inserting ΔT_{fast} (4) and (3) in Eq. (1), and by looking at the high loads asymptotic regime, we predict V to be limited by the individual heat capacity of atom bounds:

$$\begin{aligned} V_{\text{lim}} &\sim V_0 \left[1 - \exp \left(- \frac{\alpha^2 (1 + G_h/G)}{k_B (T_0/G + \phi/[\pi Cl])} \right) \right] \\ &\sim V_0 \left[1 - \exp \left(- \frac{d_0^3 C}{4 k_B \phi} \right) \right], \end{aligned} \quad (6)$$

where the crossed out terms are neglected. Note that $V_{\text{lim}} \sim 126$ m/s⁻¹ is smaller than the actual maximum crack velocity $V_{\text{max}} \sim 160$ m/s⁻¹, which is obtained for $G = G_c$.

We pursue the comparison with the reported rupture of another material, acrylic based pressure sensitive adhesives (PSA), typically happening when unrolling office tape. For Scotch[®] 3M 600 rolls, two propagation modes are indeed measured²¹, and some stick-slip is observed passed a specific velocity²⁰ $V \sim 15 \text{ cm s}^{-1}$. The full (G , V) data and model fit is shown in Fig. 3. As no significant healing threshold displays at low velocity, we assume that G_h is high enough to neglect the healing term (see the supplementary material for further discussion), and we invert the model's parameters in the same way as for PMMA. First, α is given by the slope of the slow phase: $\alpha \sim 21 \text{ pm}$. The highest velocity records gives $V_0 \sim 30 \text{ m s}^{-1}$ and the intercept at low velocity indicates $G_c \sim 146 \text{ J m}^{-2}$. Satisfyingly, V_0 compares with the mechanical wave velocity in PSA, $\sqrt{\mu/\rho}$, where μ is its shear modulus²⁴, 0.1 to 1 MPa, and ρ its volumetric mass²⁵, about 10^3 kg m^{-3} . From the local G maximum at the higher end of the slow datum, we infer λ/ϕ in the order of $0.1 \text{ Js}^{-1} \text{ m}^{-1} \text{ K}^{-1}$ and, as the adhesive's conductivity lies in the same range²⁶, a consequent portion of G should be released into heat: $\phi \sim 1$. Finally, we estimate l to be in the nanometer range, based on the coolest points of the fast phase.

We thus have shown how statistical physics, together with the dissipation and diffusion of heat, can simply explain the dynamics of both creeping and fast cracks, as well as the shifts from one state to the other. While giving valuable insights on the rupture of both media, our quantification for each model parameter stays rather approximate (i.e. we mainly derived orders of magnitude). They were indeed considered to be constant while most could be velocity or temperature dependent^{11,12,27}. We also considered PMMA and PSA as homogeneously tough while G_c is likely to present some quenched disorder. While this should not affect the stable propagation branches, as long as G and V are understood as averaged over a few G_c correlation lengths, it could be of importance for the accuracy of the phase transitions, as slow cracks shall preferentially avalanche on weaker zones and fast cracks stop on stronger locations. In the supplementary information we further illustrate

the parameters sensitivity. We predict that the release of heat is concentrated on nanometers around the tip, with ΔT reaching several thousands of degrees. Experimentally confirming this temperature on such a small scale is challenging. So is modelling it with appropriate atomistic simulations^{28,29}, as it calls for sampling frequencies higher than $V_0/d_0 \sim 10^{13} \text{ Hz}$. It is however compatible with experimental estimations in glass and quartz^{17,30,31}, obtained by characterising the photons emission from the crack tips. Similarly, when peeling tape, a blue tribo-radiation can be observed during the fast stages^{21,32} (see Fig. 3), and we point out that such coloured emission could correspond to the central frequencies associated via Wien's law³³ with a blackbody temperature compatible with our model. Furthermore, the intensity of the observed light, which is only visible in the dark, is also model consistent: we expect indeed a radiated power³³ $s(T_0 + \Delta T)^4 h l \sim 1 \text{ } \mu\text{W}$ to 1 mW , with $s = 5.67 \times 10^{-8} \text{ W m}^{-2} \text{ K}^{-4}$ the Stefan-Boltzmann constant and h the tape width ($\sim 2 \text{ cm}$). As for the area which emits the radiations, the proposed nanometers may correspond to the typical entanglement density in polymers, below which atoms have more freedom to oscillate and which is known to affect rupture properties³⁴. General elasticity⁸ predicts however plastic zones far larger, in the order of $G/(2\pi\sigma_y^2 E)$, around $100 \text{ } \mu\text{m}$ in PMMA, σ_y being the tensile yield stress and E the young modulus. Some residual heat could yet be dissipated at this scale, and l only be a core size for plasticity. $100 \text{ } \mu\text{m}$ is actually similar to the distance at which PMMA micro-cracks nucleate from the main front¹⁴. Besides, the imaging of postmortem surfaces reveals spherical cavities in their centres (see Fig. 2), which could correspond to bubbles, forming by sublimation³⁵ due to a high temperature reached on weak locations of the plastic zone, and leading to fractures once having grown to a critical size. Thus, in addition to explaining the full dynamics of singular fronts, thermal processes could be responsible for their complication at high propagation velocity. The appearance of secondary fronts, for loads passed our inferred G_c , might correspond to new dissipation processes, when cracks propagate over-critically and some extra energy is brought to the system.

-
- [1] A. Griffith. The Phenomena of Rupture and Flow in Solids. *Philosophical Transactions of the Royal Society of London A: Mathematical, Physical and Engineering Sciences*, 221(582-593):163–198, January 1921. ISSN 1471-2962. doi:10.1098/rsta.1921.0006.
 - [2] W. Döll and L. Könzöl. Micromechanics of fracture under static and fatigue loading: Optical interferometry of crack tip craze zones. In *Crazing in Polymers Vol. 2*, pages 137–214. Springer Berlin Heidelberg, 1990. ISBN 978-3-540-46192-0.
 - [3] J. Fineberg and M. Marder. Instability in dynamic fracture. *Physics Reports*, 313:1 – 108, 1999.
 - [4] S. S. Brenner. Mechanical behavior of sapphire whiskers at elevated temperatures. *Journal of Applied Physics*, 33(1):33–39, 1962. doi:10.1063/1.1728523.
 - [5] S. N. Zhurkov. Kinetic concept of the strength of solids. *International Journal of Fracture*, 26(4):295–307, Dec 1984. ISSN 1573-2673. doi:10.1007/BF00962961.
 - [6] S. Santucci, L. Vanel, and S. Ciliberto. Subcritical statistics in rupture of fibrous materials: Experiments and model. *Phys. Rev. Lett.*, 93:095505, Aug 2004. doi:10.1103/PhysRevLett.93.095505.
 - [7] A. Cochard, O. Lengliné, K. J. Måløy, and R. Toussaint. Thermally activated crack fronts propagating in pinning

- disorder: simultaneous brittle/creep behavior depending on scale. *Philosophical Transactions of the Royal Society A : Mathematical, Physical and Engineering Sciences*, 2018. doi:10.1098/rsta.2017.0399.
- [8] B. Lawn. *Fracture of Brittle Solids*. Cambridge Solid State Science Series. Cambridge University Press, 2 edition, 1993. doi:10.1017/CBO9780511623127.
- [9] D. Maugis. Subcritical crack growth, surface energy, fracture toughness, stick-slip and embrittlement. *Journal of Materials Science*, 20(9):3041–3073, Sep 1985. ISSN 1573-4803.
- [10] G. R. Irwin. Analysis of stresses and strains near the end of a crack traversing a plate. *Journal of Applied Mechanics*, 24:361–364, 1957.
- [11] G. P. Marshall, L. H. Coutts, and J. G. Williams. Temperature effects in the fracture of PMMA. *Journal of Materials Science*, 9(9):1409–1419, Sep 1974. ISSN 1573-4803. doi:10.1007/BF00552926.
- [12] G. Carbone and B. N. J. Persson. Hot cracks in rubber: Origin of the giant toughness of rubberlike materials. *Phys. Rev. Lett.*, 95:114301, Sep 2005. doi:10.1103/PhysRevLett.95.114301.
- [13] J. Scheibert, C. Guerra, F. Célarié, D. Dalmas, and D. Bonamy. Brittle-quasibrittle transition in dynamic fracture: An energetic signature. *Phys. Rev. Lett.*, 104:045501, Jan 2010. doi:10.1103/PhysRevLett.104.045501.
- [14] C. Guerra, J. Scheibert, D. Bonamy, and D. Dalmas. Understanding fast macroscale fracture from microcrack post mortem patterns. *Proceedings of the National Academy of Sciences*, 109(2):390–394, 2012. ISSN 0027-8424. doi:10.1073/pnas.1113205109.
- [15] J.R. Rice. Thermodynamics of the quasi-static growth of Griffith cracks. *Journal of the Mechanics and Physics of Solids*, 26(2):61 – 78, 1978. doi:10.1016/0022-5096(78)90014-5.
- [16] L. B. Freund. Crack propagation in an elastic solid subjected to general loading. *Journal of the Mechanics and Physics of Solids*, 20(3):129 – 152, 1972. ISSN 0022-5096. doi:10.1016/0022-5096(72)90006-3.
- [17] R. Weichert and K. Schönert. Heat generation at the tip of a moving crack. *Journal of the Mechanics and Physics of Solids*, 26(3):151 – 161, 1978. ISSN 0022-5096. doi:https://doi.org/10.1016/0022-5096(78)90006-6.
- [18] R. Toussaint, O. Lengliné, S. Santucci, T. Vincent-Dospital, M. Naert-Guillot, and K. J. Måløy. How cracks are hot and cool: a burning issue for paper. *Soft Matter*, 12:5563–5571, 2016. doi:10.1039/C6SM00615A.
- [19] L. Vanel, S. Ciliberto, P.-P. Cortet, and S. Santucci. Time-dependent rupture and slow crack growth: elastic and viscoplastic dynamics. *Journal of Physics D: Applied Physics*, 42(21):214007, oct 2009. doi:10.1088/0022-3727/42/21/214007.
- [20] M.-J. Dalbe, S. Santucci, P.-P. Cortet, and L. Vanel. Strong dynamical effects during stick-slip adhesive peeling. *Soft Matter*, 10:132–138, 2014. doi:10.1039/C3SM51918J.
- [21] M. Barquins and M. Ciccotti. On the kinetics of peeling of an adhesive tape under a constant imposed load. *International Journal of Adhesion and Adhesives*, 17(1): 65 – 68, 1997. ISSN 0143-7496. doi:10.1016/S0143-7496(96)00020-6.
- [22] M.L. Hattali, J. Barés, L. Ponson, and D. Bonamy. Low velocity surface fracture patterns in brittle material: A newly evidenced mechanical instability. In *THERMEC 2011*, volume 706 of *Materials Science Forum*, pages 920–924. Trans Tech Publications Ltd, 1 2012. doi:10.4028/www.scientific.net/MSF.706-709.920.
- [23] M. Parvin. Theoretical prediction of temperature rise at the tip of a running crack. *International Journal of Fracture*, 15(5):397–404, Oct 1979. ISSN 1573-2673. doi:10.1007/BF00023327.
- [24] C. Creton. Pressure-sensitive adhesives: An introductory course. *MRS Bulletin*, 28(6):434–439, 2003. doi:10.1557/mrs2003.124.
- [25] S. G. Robert, A. Morse, E. Siband, D. Dupin, S. P. Armes, and J. L. Keddie. Mechanical properties of a waterborne pressure-sensitive adhesive with a percolating poly(acrylic acid)-based diblock copolymer network: Effect of ph. *Journal of Colloid and Interface Science*, 448:8 – 16, 2015. doi:10.1016/j.jcis.2015.01.074.
- [26] J. K. Kim, J. W. Kim, M. I. Kim, and M. S. Song. Thermal conductivity and adhesion properties of thermally conductive pressure-sensitive adhesives. *Macromolecular Research*, 14(5):517–523, Oct 2006. ISSN 2092-7673. doi:10.1007/BF03218718.
- [27] K. Kitamura. Crack surface energy: Temperature and force dependence. *Materials Transactions*, 49(3):643–649, 2008. doi:10.2320/matertrans.MER2007238.
- [28] C. L. Rountree, Rajiv K. K., E. Lidorikis, A. Nakano, L. Van Brutzel, and P. Vashishta. Atomistic aspects of crack propagation in brittle materials: Multimillion atom molecular dynamics simulations. *Annual Review of Materials Research*, 32(1):377–400, 2002. doi:10.1146/annurev.matsci.32.111201.142017.
- [29] P. R. Budarapu, B. Javvaji, V. K. Sutrar, D. Roy Mahapatra, G. Zi, and T. Rabczuk. Crack propagation in graphene. *Journal of Applied Physics*, 118(6):064307, 2015. doi:10.1063/1.4928316.
- [30] G. N. Chapman and A. J. Walton. Triboluminescence of glasses and quartz. *Journal of Applied Physics*, 54(10): 5961–5965, 1983. doi:10.1063/1.331773.
- [31] G. Pallares, C. L. Rountree, L. Douillard, F. Charra, and E. Bouchaud. Fractoluminescence characterization of the energy dissipated during fast fracture of glass. *Europhysics Letters*, 99(2):28003, 2012.
- [32] C. Camara, J. Escobar, J. R. Hird, and S. J. Putterman. Correlation between nanosecond x-ray flashes and stick-slip friction in peeling tape. *Nature*, 455:1089–92, 11 2008. doi:10.1038/nature07378.
- [33] P. Jain and L. Sharma. The physics of blackbody radiation: A review. *Journal of Applied Science in Southern Africa*, 4:80–101, 02 1998. doi:10.4314/jassa.v4i2.16899.
- [34] C. S. Henkee and E. J. Kramer. Crazing and shear deformation in crosslinked polystyrene. *Journal of Polymer Science: Polymer Physics Edition*, 22(4):721–737, 1984. doi:10.1002/pol.1984.180220414.
- [35] H. Arisawa and T.B. Brill. Kinetics and mechanisms of flash pyrolysis of poly(methyl methacrylate) (PMMA). *Combustion and Flame*, 109(3):415 – 426, 1997. ISSN 0010-2180. doi:https://doi.org/10.1016/S0010-2180(96)00190-3.

Supplementary information is available online.

Author contributions: T.V.D. developed and analysed the model and redacted the first versions of the manuscript. R.T. proposed the physical basis of the model and its mathematical formulation. A.C. worked on its numerical implementations. D.B. and L.H. provided and advised on the PMMA data and images. S.S. and L.V. gave direct insights on the tape experiments.

K.J.M. and E.G.F. contributed in the interpretation of the model in fracture mechanics applications. All authors participated to the redaction of the manuscript and agreed with the submitted version.

Author information: Reprint and permissions information is available online. Authors declare no competing financial interests in the publishing of this work. Readers are welcome to comment and correspondence should be addressed to vincentdospitalt@unistra.fr

From thermal creeping to thermal weakening: How crushing plastic and unrolling tape unravels fracture physics

SUPPLEMENTARY INFORMATION

Tom Vincent-Dospital,^{1,2,*} Renaud Toussaint,^{1,2,†} Stéphane Santucci,^{3,4} Loïc Vanel,⁵ Daniel Bonamy,⁶ Lamine Hattali,⁷ Alain Cochard,¹ Eirik G. Flekkøy,² and Knut Jørgen Måløy²

¹*Institut de Physique du Globe de Strasbourg, UMR 7516 CNRS, Université de Strasbourg/EOST, France*

²*SFF Porelab, The Njord Centre, Department of physics, University of Oslo, Norway*

³*Laboratoire de Physique, ENS Lyon, France*

⁴*Mechanics of disordered media laboratory, Lavrentyev Institute of Hydrodynamics of the Russian Academy of Science*

⁵*University of Lyon, Université Claude Bernard Lyon 1, CNRS,*

Institut Lumière Matière, F-69622, VILLEURBANNE, France

⁶*Service de Physique de l'Etat Condensé, CEA, CNRS,*

Université Paris-Saclay, CEA Saclay, 91191 Gif-sur-Yvette Cedex, France

⁷*Laboratoire FAST, UMR 7608 CNRS, Université Paris-Sud, France*

(Dated: September 2, 2022)

CONTENTS

I. Down-scaling from the energy release rate to the tip elastic energy	1
II. Parameters sensibility for the data fit	2
III. Healing processes in tape	4
IV. Method: Measurement of crack velocity vs energy release rate in PMMA	4
References	5

I. DOWN-SCALING FROM THE ENERGY RELEASE RATE TO THE TIP ELASTIC ENERGY

We presented an Arrhenius based model which activation energy E_a is written as a function of the energy release rate G :

$$E_a = \alpha^2(G_c - G), \quad (1)$$

where α^2 is an area related to the typical size of the breaking sites and G_c the critical energy release rate above which the sites of a given surface break. This law fits well observed crack dynamics¹, but for a value of α which is however less than the typical inter-atomic distance (i.e., about an ångström), making its physical meaning questionable. It was proposed² that for a crack to advance by a nominal surface, several off-plane bonds have to be broken, and hence that α holds a projective information. Vanel et al.³ proposed another reason for

α to be an ad hoc scale: the sub-critical growth rate is to be written at the microscopic scale, rather than using the macroscopic G . If we consider the link undergoing the rupture process to be elastic and that it breaks passed a critical elastic energy, we can then write the Arrhenius activation energy as:

$$E_a = d_0^3 \left(\frac{\sigma_c^2}{2E} - \frac{\sigma_{\text{tip}}^2}{2E} \right), \quad (2)$$

where σ_{tip} is the stress at the tip of the crack, σ_c the rupture threshold, d_0^3 the characteristic volume of the link ($d_0 \sim 1 \text{ Å}$), and E an elastic modulus, say the Young modulus for cracks that open in mode I. To scale (2) back to (1), we use the general elasticity theory⁴, predicting that the stress around a crack tip is governed by:

$$\sigma(r) \sim \frac{K}{\sqrt{2\pi r}}, \quad (3)$$

where K is the fracture toughness, $G \sim K^2/E$, and r is the distance to the tip. While this expression diverges for $r \rightarrow 0$, it is considered⁵ that the tip is shielded by its surrounding plastic zone, in which most energy is dissipated, and the actual stress is then constrained by the radius l of this zone:

$$\sigma_{\text{tip}} \sim \sqrt{\frac{GE}{2\pi l}}. \quad (4)$$

Often, such stress at the tip is considered to be fixed at a characteristic yield value, with variations in G that are balanced by variations in l . In our model, however, we have considered l to be constant, such that σ_{tip} increases with G . Inserting Eq. (4) into (2) and comparing with (1), an expression is deduced for the α parameter³:

$$\alpha \sim \sqrt{\frac{d_0^3}{4\pi l}}. \quad (5)$$

* vincentdospital@unistra.fr

† renaud.toussaint@unistra.fr

With d_0 in the order of 0.1 nm, and with l in the nanometer range as discussed in the main letter, Eq. (5) predicts α to be about 10 pm, compatible with the values inferred from the slow velocity branches of the tape and the PMMA data. The model is hence satisfyingly self-consistent. Note that we have defined l as the scale at which most of the Joule heating is introduced. However, it could only be a core size for the plasticity, rather than its full extent, and residual energy dissipation might occur further from the tip (i.e., for $r > l$). We have thus assumed that expression (3) approximately holds despite such residual plasticity.

If not assuming perfectly elastic bonds between atoms (i.e., Eq. (2)), the relation between the stress and the energy release rate can still generally be written as:

$$G = \int_{d_0}^d \sigma(d') dd', \quad (6)$$

d_0 being the nominal separation of atoms in an unloaded matrix (i.e., at $G = 0$) and d the actual atom separation at the crack tip. Figure 1 illustrates this relation, as well as how the thermal bath allows to overcome the energy barriers, G_c and G_h .

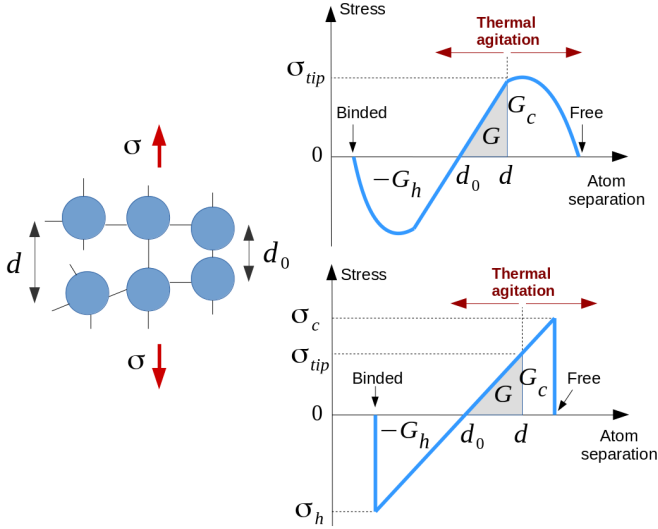


FIG. 1. Left: simplified atomic view of the breaking/healing site at the crack tip. Top right: generic stress to atom separation function. Bottom right: stress to atom separation function for an elastic bond, as considered by Eq. (2). The function slope depends on the young modulus E and on the radius of the shielding zone l . G is the grey area, G_c the area below the curve for $d > d_0$ and G_h the area for $d < d_0$.

II. PARAMETERS SENSIBILITY FOR THE DATA FIT

We here show, on the PMMA data, how varying the model's parameters around their inferred values impacts the model fit, thus giving the reader a better feeling for their individual effect and sensitivity. In figures 2 to 8, a unique parameter of the model varies while the others are kept to the values used for the fit presented in the main manuscript: $\alpha = 8.3$ pm, $V_0 = 880$ m s⁻¹, $G_c = 1275$ J m⁻², $G_h = 650$ J m⁻², $\phi = 20\%$, $\lambda = 0.18$ J s⁻¹ m⁻¹ K⁻¹, $Cl = 1.5 \times 10^{-3}$ J m⁻² K⁻¹ and $T_0 = 296$ K. The plots show the data up to the apparition of the secondary micro-cracks, after which the model does not apply as such.

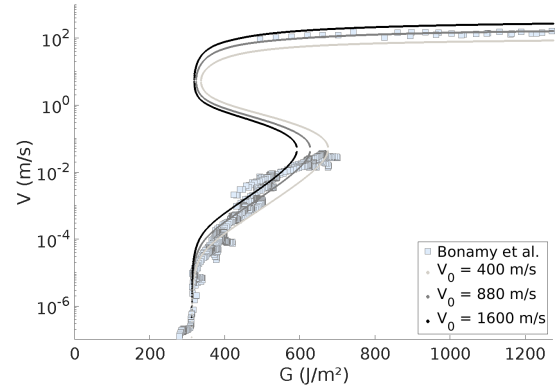


FIG. 2. Effect of varying the nominal velocity, V_0 , on the fit to the PMMA data. The propagation velocity is roughly proportional to V_0 , but also modifies the positions of the phase transitions.

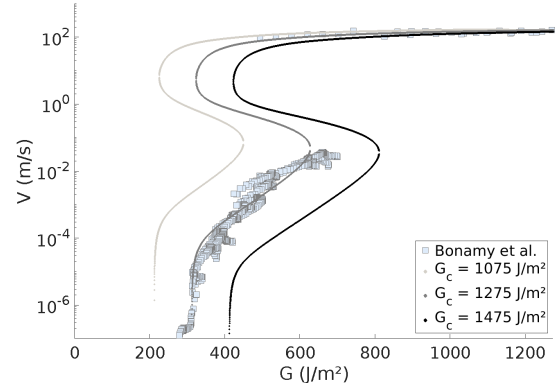


FIG. 3. Effect of varying the breaking energy barrier, G_c , on the fit to the PMMA data. At a given load, the higher G_c , the slower the crack. The transitions between the three propagation modes (fast, slow, and dominated by healing) are also affected: a medium with a stronger barrier needs a heavier load to transit to a weaker state.

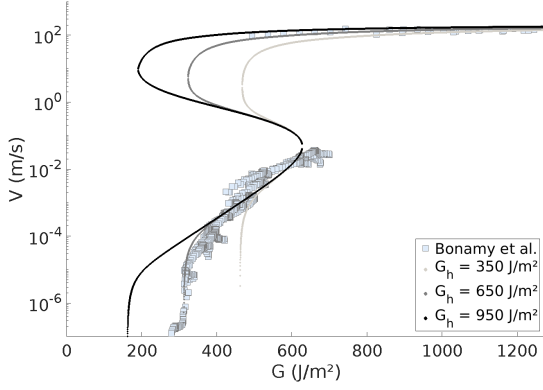


FIG. 4. Effect of varying the healing energy barrier, G_h , on the fit to the PMMA data. A crack that heals more easily needs a higher load to actually propagate forward or to stay in the high velocity regime.

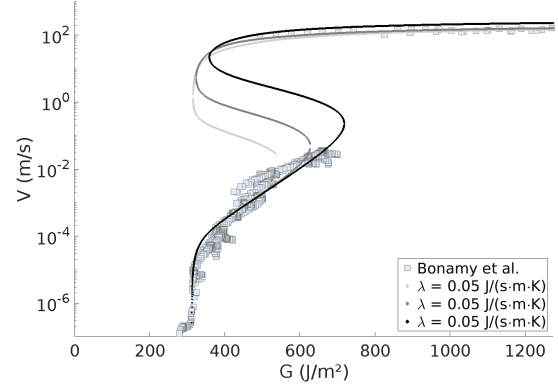


FIG. 7. Effect of varying the thermal conductivity, λ , on the fit to the PMMA data. With higher λ , the heat is better evacuated: the slow to fast branch threshold shifts towards higher G and V . The fast regime is not sensitive to λ , as ΔT is there constrained by l .

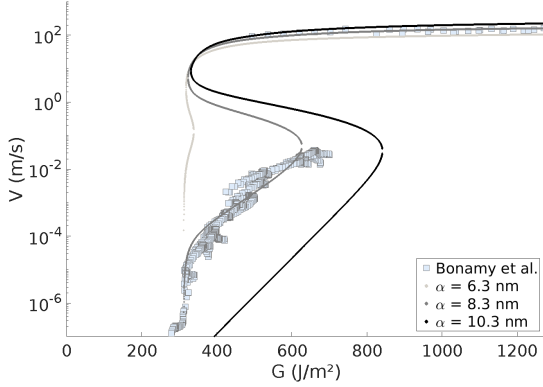


FIG. 5. Effect of varying the characteristic size of a breaking link, α , on the fit to the PMMA data. α mainly controls the slope and the intercept of the low velocity branch. A small change in α significantly modifies this branch as well as the threshold to the fast regime.

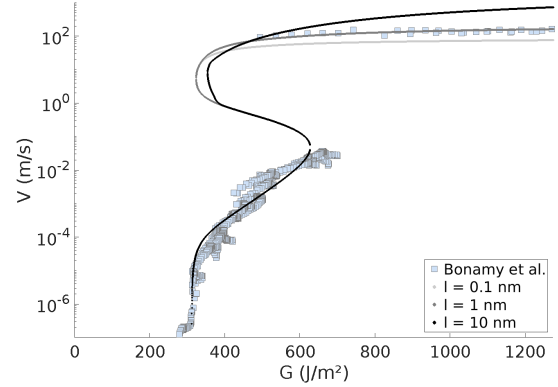


FIG. 8. Effect of varying the process zone radius, l , on the fit to the PMMA data. l mainly impacts the plot curvature on the high velocity branch. No effect is observed on the slow branch as the thermal elevation is there constrained by the diffusion skin depth rather than by the plasticity scale.

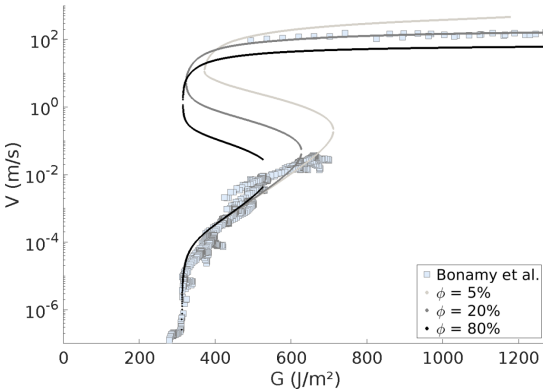


FIG. 6. Effect of varying the ratio of energy converted to heat, ϕ , on the fit to the PMMA data. The maximum velocity increases with ϕ as the tip temperature is higher. The threshold from the slow to the fast branch shifts towards lower G as a lighter load is required for the temperature to significantly deviate from T_0 .

Investigating the relative sensitivity of each parameter, we thus assess the uncertainty of their inverted value, which is: a few picometers for α and a few nanometers for l , about 10% for ϕ , a few hundreds of Joules per square meter for G_c and G_h , and V_0 assumed to be in the order of the mechanical waves velocities. To this relatively high uncertainties, adds up the experimental inaccuracy for V and G , as well as the limitation of our very first order physical model. Still, the data is overall well explained over eight decades of velocities, for several materials and with parameters that are in credible orders of magnitude.

III. HEALING PROCESSES IN TAPE

In our letter, we considered the healing processes to be negligible in order to describe the dynamics of unrolling tape, as no low velocity constant G asymptote arising from crack healing displays in the (G, V) data. We here temper this assertion by showing fits that do not disregard their effect (i.e., we do not assume $G_h \gg G_c$). Indeed, the asymptote could be present, but at a load smaller than the measured ones, or even at a negative load (when compressing the medium). The latter happens if G_c is smaller than G_h , as the asymptote is obtained for $[G_c - C_h]/2$. Thus, the healing energy barrier could still be comparable to the breaking one, and so significantly impact the high velocity propagation branch, when the crack tip is hot enough. Of course, an accurate quantification of this effect suffers from the absence of the asymptote as it is a good constrain for G_h . Figure 9 still shows a model not disregarding healing, and compares it with the tape data. The match is improved compared to the fit presented in the main manuscript as we have here an additional degree of freedom. The parameters are as follow: $\alpha = 21$ pm, $V_0 = 70$ m s⁻¹, $G_c = 154$ J m⁻², $G_h = 200$ J m⁻², $\phi = 60\%$, $\lambda = 0.3$ J s⁻¹ m⁻¹ K⁻¹, $Cl = 10^{-3}$ J m⁻² K⁻¹ and $T_0 = 296$ K.

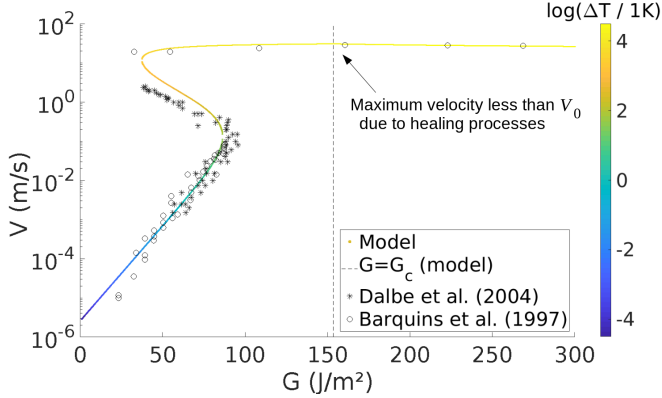


FIG. 9. Fit of the Scotch® 3M 600 data^{6,7} with a model including healing processes. The unstable (middle) branch of the model should not necessarily match the data point which are averaged G and V values for a front that stick-slips.

Note that Barquins et al.⁸, who released part of the data presented in Fig. 9, also provided similar measurements for another type of roller tape, Scotch® 3M 602. For this new medium, the (V, G) cross-plot at low velocity do call for healing processes, as shown in Fig. 10, and we then propose a fit with the following parameters: $\alpha = 10$ pm, $V_0 = 200$ m s⁻¹, $G_c = 500$ J m⁻², $G_h = 480$ J m⁻², $\phi = 60\%$, $\lambda = 0.3$ J s⁻¹ m⁻¹ K⁻¹, $Cl = 10^{-3}$ J m⁻² K⁻¹ and $T_0 = 296$ K.

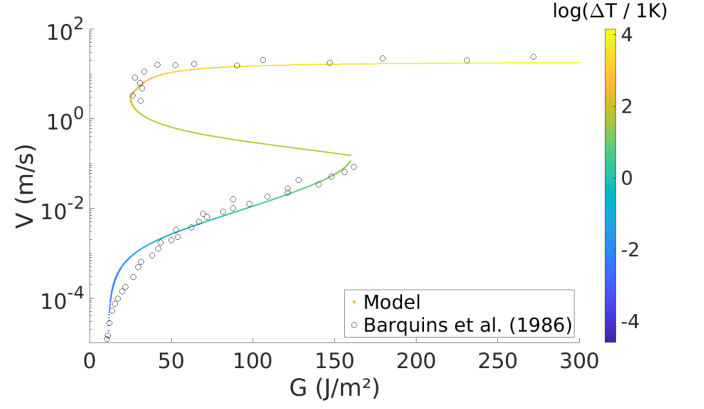


FIG. 10. Fit of the Scotch® 3M 602 data⁸. The lack of linearity at low velocity calls for healing processes in our model. Note also the curvature on the lower end of the high velocity branch, not present in the other data sets that we show but compatible with our model.

IV. METHOD: MEASUREMENT OF CRACK VELOCITY VS ENERGY RELEASE RATE IN PMMA

Wedge splitting fracture tests were used to measure both the slow and fast $V(G)$ branches in PMMA^{9,10}. Rectangular plates of size $140 \times 125 \times 15$ mm³ are first machined from a plate of moulded PMMA (Perspex®). A 25×25 mm² notch is subsequently cut out on one of the two lateral edges and a 8 mm long 800 μ m thick groove is finally introduced in the middle of the notch with a diamond saw.

To grow slow cracks, an additional seed crack (~ 2 mm-long) was added at the end of the groove via a razor blade. This crack is loaded in tension by pushing a steel wedge (semi-angle of 15°) in the notch. Two steel blocks equipped with rollers are placed in between the wedge and the specimen notch to limit the parasitic mechanical dissipation through plastic deformations or friction at loading contacts. As a result, the vicinity of the crack tip can be assumed to be the sole dissipation source for mechanical energy in the system. The wedge speed is first set to 1.6μ m s⁻¹. The force F applied by the wedge to the specimen increases linearly with time up to a point F_c above which the seed crack starts to propagate. Above this point, F decreases with time. We let the crack propagate over a distance of about 10 mm. This ensures reproducible initial conditions with a long-enough well-defined sharp seed crack. The specimen is then unloaded (unloading wedge speed: 16μ m/s). The specimen is then loaded again at a constant prescribed wedge speed V_{wedge} , which has been varied from 1.6μ m/s to 1.2 mm/s. For $V_{\text{wedge}} < 300 \mu$ m s⁻¹, stable, continuous, crack growth is observed all along the experiment up to the complete breakdown of the specimen. Above 300μ m s⁻¹, the dynamics is intermittent, with successive phases of fast growth¹⁰ interspersed with periods of slow

growth.

During each fracture test, the force $F(t)$ is monitored in real-time via a cell force mounted on the system (S-type Vishay load cell, maximum force of 100 N, measured accuracy of 1 N at 50 kHz acquisition rates, and 0.001 N at 1 Hz). A camera (USB2 uEye from IDS Imaging Development) is also used to image crack propagation at the specimen surface, (space and time accuracy of 125 μm and 0.1 s). A coarse approximation of the crack speed can be obtained by differentiating the position of the crack tip observed on the successive images. However, a more accurate signal $V(t)$ is obtained from the force signal (see Barés et al.¹¹ for details on the method). Indeed, in a linear elastic isotropic material like PMMA, the specimen stiffness $k(t) = F(t)/(V_{\text{wedge}}t)$ is a continuous decreasing function of the crack length, $c(t)$, that is set by the specimen geometry only. This function has been obtained using finite element calculations on the exact experimental geometry (Cast3M software, 2D simulation assuming plane stress conditions); it was checked that the obtained k vs c curve coincides with the experimental curves obtained by plotting $k(t)$ as a function of the crack length measured by the camera. The idea is then to use this curve $k(c)$ to infer the time evolution of crack length from the signal $F(t)$: $c(t) = k^{-1}(F(t)/[V_{\text{wedge}}t])$. Time derivation of the so-obtained $c(t)$ provides a signal $V(t)$ about 50 times less noisy than that directly obtained from the camera images. The knowledge of $c(t)$ and $F(t)$ also allows determining the time evolu-

tion of elastic energy release, $G(t)$. Indeed, the total amount of mechanical energy provided to the specimen is $F^2(t)/[2k(c(t))]$. Differentiating this stored energy with respect to c directly provides $G(t)$. The plot of $V(t)$ as a function of $G(t)$ provides the different points observed in the slow stable phase of figure 2 in the main text. Twelve fracture experiments are gathered there and differ by their V_{wedge} value: 1.6 nm s^{-1} , 32 nm s^{-1} , 400 nm s^{-1} , 800 nm s^{-1} , 1.6 $\mu\text{m s}^{-1}$, 4 $\mu\text{m s}^{-1}$, 8 $\mu\text{m s}^{-1}$, 16 $\mu\text{m s}^{-1}$, 40 $\mu\text{m s}^{-1}$, 80 $\mu\text{m s}^{-1}$, 160 $\mu\text{m s}^{-1}$, 240 $\mu\text{m s}^{-1}$ and 320 $\mu\text{m s}^{-1}$.

To grow fast cracks and measure $V(G)$ in the fast stable phase, the seed crack has been replaced by a hole of tunable radius (1 to 4 mm) drilled at the end of the groove⁹. This delays fracture and increases the potential energy stored in the specimen at the initiation of crack growth. The time evolution of $V(t)$ is measured by monitoring, via an oscilloscope, the successive rupture of parallel 500 μm large metallic lines (Chromium/Gold) deposited on the surface and that of the quasi static stress intensity factor is obtained via finite element analysis (see Scheibert et al.⁹ for details). The time evolution of the mechanical energy release rate is then deduced: $G = K^2/E$ where the Young modulus E in our PMMA have been measured to be $E = 2.8 \text{ GPa}$. The plot of $V(t)$ as a function of $G(t)$ provides the different points observed in the fast stable phase of figure 2 in the main text. Five fracture experiments are gathered there and differ by the amount of stored elastic energy at crack growth initiation: 2.0 J, 2.6 J, 2.9 J, 3.8 J and 4.2 J.

-
- [1] A. Cochard, O. Lengliné, K. J. Måløy, and R. Toussaint. Thermally activated crack fronts propagating in pinning disorder: simultaneous brittle/creep behavior depending on scale. *Philosophical Transactions of the Royal Society A : Mathematical, Physical and Engineering Sciences*, 2018. doi:10.1098/rsta.2017.0399.
 - [2] O. Lengliné, R. Toussaint, J. Schmittbuhl, J. E. Elkhoury, J. P. Ampuero, K. T. Tallakstad, S. Santucci, and K. J. Måløy. Average crack-front velocity during subcritical fracture propagation in a heterogeneous medium. *Phys. Rev. E*, 84:036104, Sep 2011. doi:10.1103/PhysRevE.84.036104.
 - [3] L. Vanel, S. Ciliberto, P.-P. Cortet, and S. Santucci. Time-dependent rupture and slow crack growth: elastic and viscoplastic dynamics. *Journal of Physics D: Applied Physics*, 42(21):214007, oct 2009. doi:10.1088/0022-3727/42/21/214007.
 - [4] B. Lawn. *Fracture of Brittle Solids*. Cambridge Solid State Science Series. Cambridge University Press, 2 edition, 1993. doi:10.1017/CBO9780511623127.
 - [5] G. R. Irwin. Analysis of stresses and strains near the end of a crack traversing a plate. *Journal of Applied Mechanics*, 24:361–364, 1957.
 - [6] M.-J. Dalbe, S. Santucci, P.-P. Cortet, and L. Vanel. Strong dynamical effects during stick-slip adhesive peeling. *Soft Matter*, 10:132–138, 2014. doi:10.1039/C3SM51918J.
 - [7] M. Barquins and M. Ciccotti. On the kinetics of peeling of an adhesive tape under a constant imposed load. *International Journal of Adhesion and Adhesives*, 17(1):65 – 68, 1997. ISSN 0143-7496. doi:https://doi.org/10.1016/S0143-7496(96)00020-6.
 - [8] M. Barquins, B. Khandani, and D. Maugis. Propagation saccadée de fissure dans le pelage d’un solide viscoélastique. *Compte Rendu de l’Académie des Sciences Paris*, 303:1575–1519, 1 1986.
 - [9] J. Scheibert, C. Guerra, F. Célarié, D. Dalmas, and D. Bonamy. Brittle-quasibrittle transition in dynamic fracture: An energetic signature. *Phys. Rev. Lett.*, 104: 045501, Jan 2010. doi:10.1103/PhysRevLett.104.045501.
 - [10] M.L. Hattali, J. Barés, L. Ponson, and D. Bonamy. Low velocity surface fracture patterns in brittle material: A newly evidenced mechanical instability. In *THERMEC 2011*, volume 706 of *Materials Science Forum*, pages 920–924. Trans Tech Publications Ltd, 1 2012. doi:10.4028/www.scientific.net/MSF.706-709.920.
 - [11] J. Barés, M. L. Hattali, D. Dalmas, and D. Bonamy. Fluctuations of global energy release and crackling in nominally brittle heterogeneous fracture. *Physical Review Letters*, 113(26), dec 2014. doi:10.1103/physrevlett.113.264301. URL <http://dx.doi.org/10.1103/PhysRevLett.113.264301>.